nature chemistry

ARTICLES

PUBLISHED ONLINE: 20 JULY 2014 | DOI: 10.1038/NCHEM.2004

Controlling epithelial sodium channels with light using photoswitchable amilorides

Matthias Schönberger[1], Mike Althaus[2], Martin Fronius[2,3], Wolfgang Clauss[2] and Dirk Trauner[1]*

Amiloride is a widely used diuretic that blocks epithelial sodium channels (ENaCs). These heterotrimeric transmembrane proteins, assembled from β, γ and α or δ subunits, effectively control water transport across epithelia and sodium influx into non-epithelial cells. The functional role of δβγENaC in various organs, including the human brain, is still poorly understood and no pharmacological tools are available for the functional differentiation between α- and δ-containing ENaCs. Here we report several photoswitchable versions of amiloride. One compound, termed PA1, enables the optical control of ENaC channels, in particular the δβγ isoform, by switching between blue and green light, or by turning on and off blue light. PA1 was used to modify functionally δβγENaC in amphibian and mammalian cells. We also show that PA1 can be used to differentiate between δβγENaC and αβγENaC in a model for the human lung epithelium.

The epithelial sodium channel (ENaC) is a constitutively open sodium-selective ion channel that lacks voltage sensitivity and mediates sodium absorption across various epithelia[1]. Classical ENaCs are heterotrimers composed of three subunits, α, β and γ, which assemble as a sodium-selective ion channel in the plasma membrane (Fig. 1)[2,3]. In renal epithelia, ENaCs mediate Na^+ reabsorption by the kidney and are involved in maintaining extracellular volume and blood pressure. Gain-of-function mutations cause a hereditary form of hypertension (Liddle syndrome), whereas loss-of-function mutations give rise to the salt-wasting syndrome pseudohypoaldosteronism type 1[4,5]. ENaC-mediated sodium absorption by the pulmonary epithelium drives lung liquid clearance and is thus a critical regulator of pulmonary water content. Increased ENaC activity in the airways is the cause of cystic-fibrosis-like lung disease, whereas decreased ENaC activity in the distal lung leads to impaired alveolar fluid clearance and the development of pulmonary oedema[6–9]. As such, ENaCs are a primary target for drugs that affect electrolyte and water homeostasis, such as diuretics or oedema medications[10–13].

An additional ENaC-subunit, δ, was identified in 1995[14]. There is only scarce knowledge about its physiological function; however, it can assemble with the β and γ subunits to form channels with a high open probability[14–16]. Expression of δENaC (and other ENaCs) has been confirmed in various non-epithelial tissues, most prominently the central nervous system of primates[17–20]. It has been speculated that δ-containing ENaCs play a role in communicating ischaemic and hypoxic signals in neurons, as well as in adjusting nervous excitability[21,22]. Complicating the analysis, rodents do not appear to have a gene for the δ subunit. Furthermore, no pharmacological tools are available for functional differentiation between α- and δ-containing ENaCs. Thus, in contrast to αβγENaC, little is known about the physiological function of δβγENaC and, in particular, the function of δENaC in the brain[22].

ENaCs belong to a large group of ion channels, the ENaC/degenerin (ENaC/deg) protein family, which also includes neuronal acid-sensing ion channels[23]. Recently, the latter were elucidated with X-ray crystallography, which confirmed a trimeric architecture that probably applies to all channels of the family (Fig. 1)[24]. Every individual ENaC subunit comprises only two transmembrane helices (TM1 and TM2) with relatively short intracellular C and N termini and a large, cysteine-rich extracellular domain.

Although ENaC/deg channels respond to a variety of input signals, none are inherently sensitive towards light. In recent years, our group succeeded in developing a range of synthetic photoswitches that can confer light sensitivity to native or slightly modified receptor proteins. These can either function as freely diffusible photochromic ligands (PCLs) or as photoswitchable tethered ligands, which are covalently attached to the target protein[25]. Using either strategy, effectively we were able to turn a variety of ion channels and G-protein-coupled receptors into photoreceptors[26–30].

We now show that an entirely new class of transmembrane proteins, namely trimeric ENaC/deg channels, are amenable to the PCL approach. To this end we have designed, synthesized and characterized a small series of photoswitchable azobenzene derivatives of amiloride and identified one candidate that can be used primarily to control δβγENaC activity with light. Our photochromic ligands provide insights into the structure–activity relationships of ENaC blockers and could be used to discriminate functionally between isoforms.

Results and discussion

Design and synthesis of photoamilorides. Amiloride was introduced as a potassium-sparing diuretic in the 1960s without particular knowledge of its molecular target[31]. Subsequently, ENaC in kidney epithelia was established as the ion channel primarily responsible for the potassium-sparing diuretic effect[3]. To date, countless amiloride analogues have been synthesized and tested, which has provided insights into its structure–activity relationships[32,33]. Most importantly, it has been found that lipophilic substitution at the terminal guanidine nitrogen boosts both potency and selectivity for ENaC. Indeed, the potency gained by an aromatic substituent increases with linker length (Fig. 1b)[34]. Accordingly, we designed photochromic amiloride derivatives that have an azobenzene unit attached directly to the guanidine, which gave photoamiloride-1 (**PA1**) and photoamiloride-2 (**PA2**), both of which resemble the drug phenamil (Fig. 1). Phenamil is a long-lasting blocker of ENaCs and has been used to determine channel density[35]. In addition, we

[1]Department of Chemistry and Center for Integrated Protein Science, Ludwig Maximilians-Universität München, Butenandtstraße 5–13 (F4.086), 81377 Munich, Germany, [2]Institute of Animal Physiology, Justus Liebig University Giessen, Heinrich-Buff-Ring 26, 35392 Giessen, Germany, [3]Department of Physiology, University of Otago, PO Box 913, Dunedin 9054, New Zealand. *e-mail: dirk.trauner@lmu.de

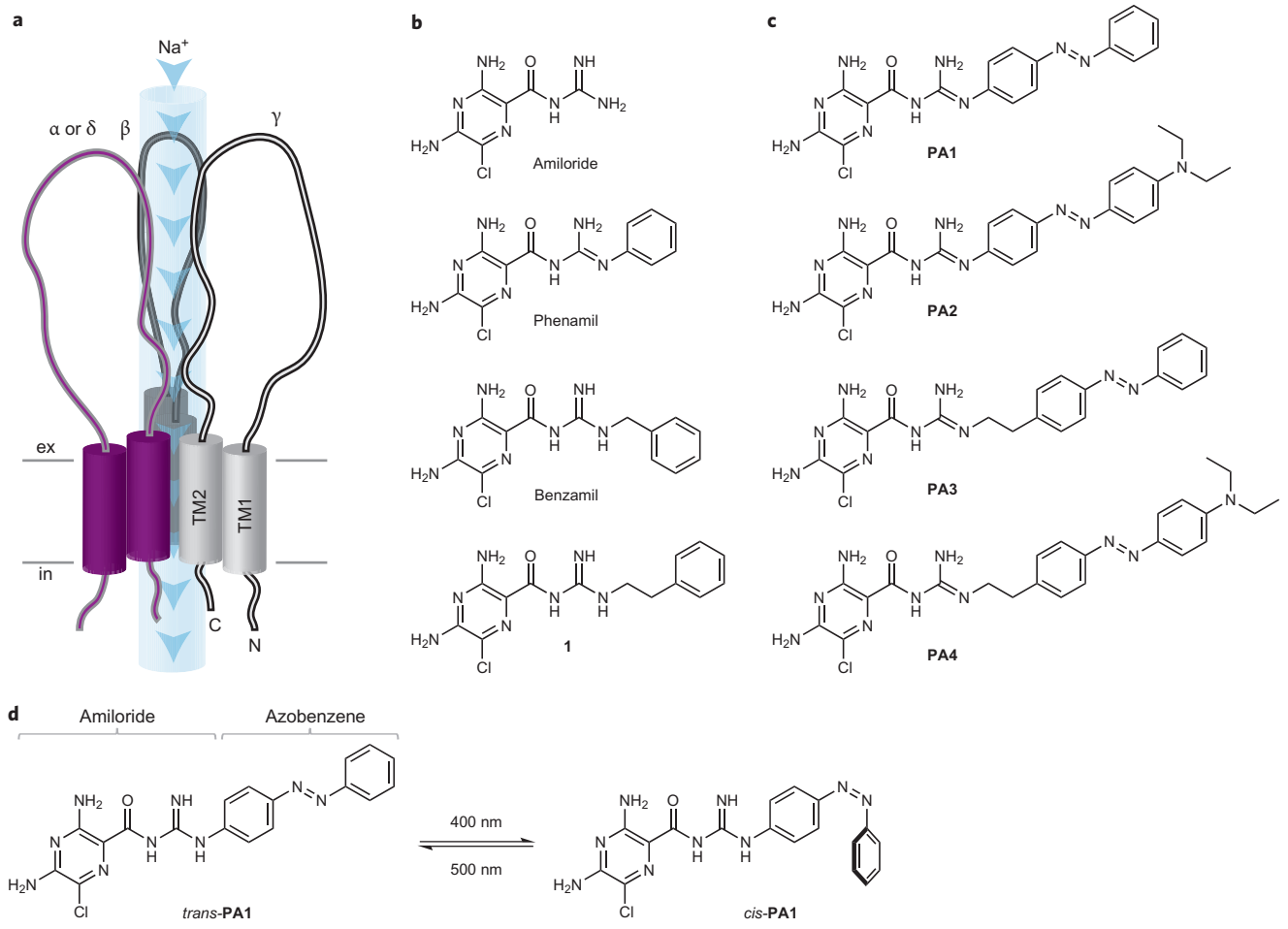

Figure 1 | ENaCs and their blockers. a, Schematic drawing of heterotrimeric αβγENaC and δβγENaC. Each subunit contains two transmembrane helices TM1 and TM2, relatively short C and N termini at the intracellular (in) site and a large extracellular (ex) loop. Under physiological conditions, ENaCs allow for a constant influx of sodium into the cell (indicated by blue arrows). **b**, Chemical structure of amiloride and its more potent derivatives phenamil, benzamil and compound **1**. **c**, Structures of photoswitchable amiloride derivatives that contain an azobenzene functional group. **d**, Photoisomerization of **PA1**. Illumination with 400 nm induces isomerization to *cis*-**PA1**, which is the thermodynamically less-stable form. The *cis* isomer can relax back to the *trans* state thermally, or, more rapidly, by illumination using 500 nm radiation.

designed the compounds photoamiloride-3 (**PA3**) and photoamiloride-4 (**PA4**), which bear an azobenzene moiety linked through an ethylene spacer and resemble the known amiloride analogue **1**[36]. In **PA2** and **PA4**, the azobenzenes are substituted further in the 4′-position with a diethylamino substituent, which is known to red shift the action spectra of azobenzenes[37]. The photoswitching of **PA1** between its *trans* and *cis* configuration is shown in Fig. 1d.

The synthesis of the shorter photoamilorides **PA1** and **PA2** started with aminoazobenzenes **2** and **3**, respectively, which were converted into aryl guanidines using cyanamide (Fig. 2a and Supplementary Information). The resulting guanidine hydrochlorides were deprotonated and condensed with an active ester of pyrazinic acid **4**, which yielded **PA1** and **PA2**, respectively.

To generate the longer photoamilorides, aniline **5** was condensed with nitrosobenzene and subsequently deprotected to yield **6** (Fig. 2b and Supplementary Information). Alternatively, oxidation of **5** and condensation with *p*-(diethylamino)aniline, followed by deprotection, gave azobenzene **7**. With these two building blocks in hand, the guanidine moiety was installed using carboxamidine **8**. The resulting guanidinium salts were deprotonated via a basic work-up and added directly to an ethanolic solution of ester **9**. Heating to reflux then yielded **PA3** and **PA4**, respectively. Interestingly, attempts to furnish **PA3** or **PA4** under the same coupling conditions as **PA1** and **PA2** (and *vice versa*) failed. Similarly, attempts to condense 4-aminoazobenzenes **2** and **3** with carboxamidine **8** did not yield the corresponding guanidines.

A single-crystal X-ray structure of **PA1** is shown in Fig. 2c. It provides the first structural data of an amiloride derivative substituted at the terminal guanidine nitrogen and reveals an extended hydrogen-bonding network that involves an amine on the pyrazine, the adjacent carbonyl and the guanidine (dotted lines).

Photophysical characterization of photoamilorides. To determine absorption maxima and the optimal wavelengths for photoswitching, solutions of **PA1-4** (50 μM, dissolved in dimethylsulfoxide (DMSO) were irradiated at different wavelengths using a monochromator (Till Photonics Polychrome 5000, Supplementary Fig. 1). DMSO was chosen as the solvent to slow down the thermal relaxation to resolve the absorption spectra of *cis* and *trans* isomers for red-shifted candidates[38]. Thus, it was possible to identify wavelengths that led to the highest *cis* and *trans* content for each molecule (Fig. 2d).

Electrophysiological characterization of photoamilorides in the dark. To identify the amiloride derivative that would be the best photochromic ENaC blocker, initially we performed microelectrode recordings on *Xenopus* oocytes that express

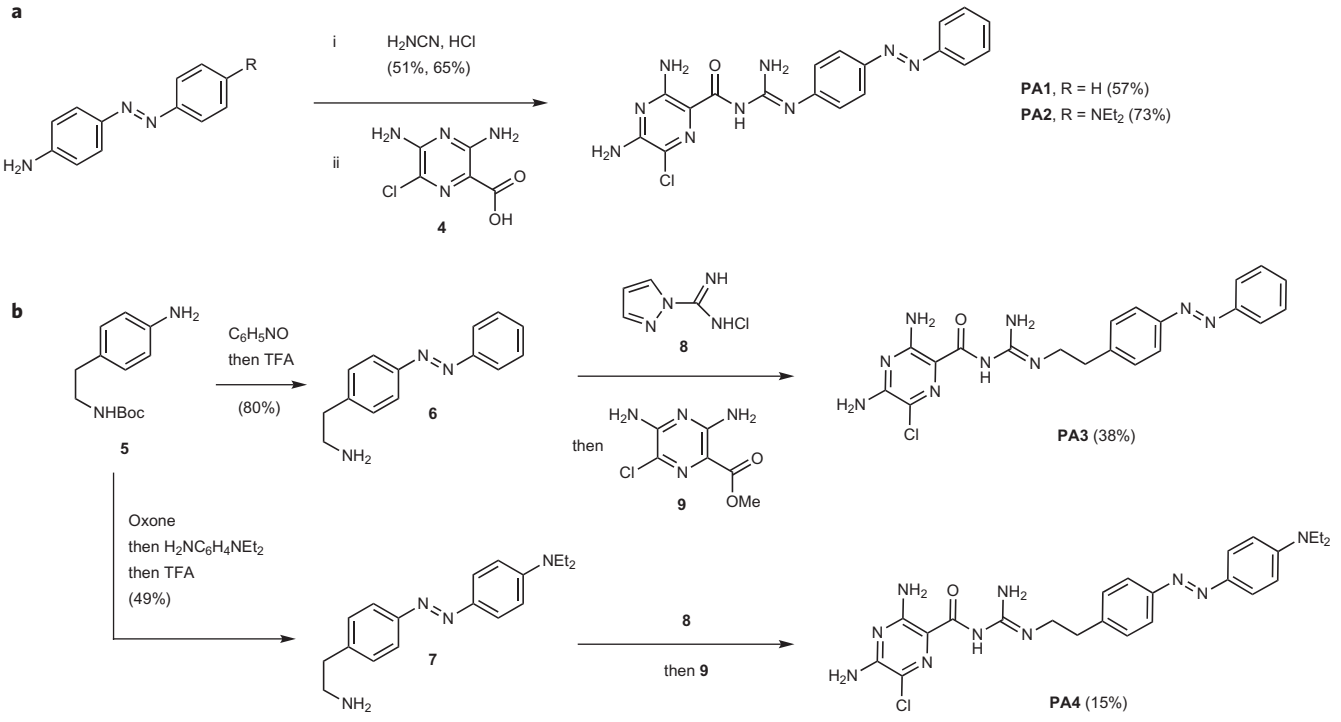

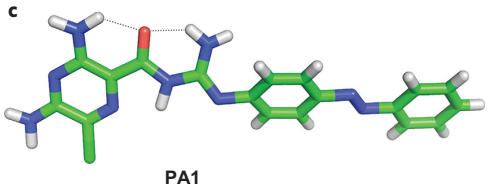

d

	Switching wavelengths (nm)	
	λ (*cis*)	λ (*trans*)
PA1	400	500
PA2	440	600
PA3	360	500
PA4	420	560

e

	IC_{50} values (nM)		
	αβγ	δβγ	δ/α
PA1	90	390	4.3
PA2	346	8,000	23.1
PA3	36	80	2.2
PA4	4	14	3.5

Figure 2 | PA synthesis and characterization. a, Synthesis of **PA1** and **PA2** starts with 4-aminoazobenzenes **2** and **3**, respectively. Reaction with cyanamide installs guanidine functional groups, which can be coupled with an active ester of **4** to yield **PA1** and **PA2**. **b**, Synthesis of **PA3** and **PA4** starts from the protected phenethylamine **5**, which can be either condensed with nitrosobenzene or oxidized to a nitrosobenzene and condensed with *p*-(diethylamino) aniline. After acidic deprotection, primary amine building blocks **6** and **7** are functionalized to guanidines, which can react with ester **9** to yield **PA3** and **PA4**, respectively. **c**, X-ray structure of **PA1** indicates an extended hydrogen-bond network (dotted lines). **d**, Optimal wavelengths for photoswitching were determined using UV/vis spectroscopy. Generally, the more conjugated candidates **PA1** and **PA2** are more red-shifted than their corresponding homologues **PA3** and **PA4**. Substitution with the electron-donating diethylaniline functionality leads to a red shift compared to the unsubstituted candidates (**PA2** and **PA4** versus **PA1** and **PA3**). **e**, IC_{50} values of **PA**s in their dark-adapted *trans* form. **PA4** is the most-potent and **PA2** is the least-potent ENaC blocker. All **PA** molecules are more potent on the αβγ isoform. **PA2** discriminates the most between αβγENaC and δβγENaC.

human αβγENaC and δβγENaCs for all the molecules (Supplementary Fig. 2). In the presence of a dim room light to ensure that **PA**s were in their *trans* form, a series of increasing ligand concentrations was applied, followed by full block using a 100 μM amiloride solution. This enabled both the determination of half-maximum inhibitory concentration (IC_{50}) values and a relative block compared to the full blocker amiloride (Fig. 2e and Supplementary Fig. 2). It was found that all the photochromic ligands synthesized were ENaC blockers. In general, they have a higher affinity for α-containing than δ-containing ENaCs. **PA4** is the most potent molecule with IC_{50} values of 4 and 14 nM for αβγENaC and δβγENaC, respectively. The weakest blocker is **PA2** with IC_{50} values of 346 and 8,000 nM for αβγENaC and δβγENaC, respectively. For comparison, amiloride has IC_{50} values of 100 nM and 2,600 nM on αβγENaC and δβγENaC channels, respectively, in a similar experimental setting.[22]

The structure–activity relationships of our small molecular series provided additional interesting findings (Fig. 2e). Matching the pharmacology of previously known ENaC blockers, the addition of a C-2 linker markedly increased affinity, as **PA3** and **PA4** are substantially more potent than their shorter analogues. The addition of a substituent in the 4′-position in **PA4** further increased potency compared to the unsubstituted **PA3**. However, this trend is reversed when there is no linker between the guanidine and the azobenzene moiety.

Photocurrents in *Xenopus* oocytes. To investigate which compound elicits the most-pronounced photoeffect, we performed electrophysiological recordings on *Xenopus* oocytes that expressed either αβγENaC or δβγENaC in combination with monochromatic illumination. **PA1**–**PA4** were applied at varying concentrations and the illumination wavelengths were switched in intervals of one minute as the perfusion was stopped (Supplementary Fig. 3). Among our four amiloride derivatives, **PA1** emerged as the most-efficient photochromic blocker, especially when applied to the δβγ isoform. Our further investigations therefore focused on this compound. As shown in Fig. 3, illumination of **PA1** with 400 nm radiation immediately

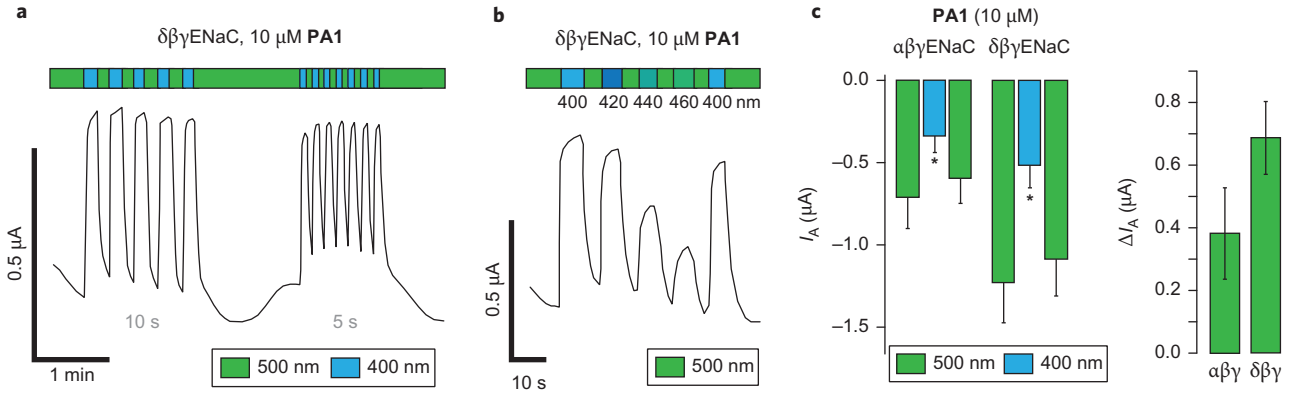

Figure 3 | PA1 photoswitching in *Xenopus* oocytes. a, Reversible block of δβγENaC currents evoked by photoisomerization of **PA1** (10 μM) in 10 s and 5 s intervals. **b**, Action spectrum of **PA1**. Wavelengths were switched between 500 nm and 400 + *x* nm (*x* = 0, 20, 40, 60). The largest photoswitchable currents are observed when 500 and 400 nm are used as illumination wavelengths for *cis* and *trans* isomerization. **c**, Photoswitching of **PA1** tested on an amiloride-sensitive current (I_A) of αβγENaC-expressing (left) and δβγENaC-expressing (right) *Xenopus* oocytes by two-electrode voltage clamp recordings. Perfusion was stopped and illumination wavelengths were switched between 500 and 400 nm in one minute intervals. Current values were taken at the end of each interval and averaged (*n* = 12 and 10, respectively). Error bars indicate s.e.m., and significance refers to switching from 400 nm to 500 nm (*$p < 0.05$). There is a reversible photoswitching effect on both αβγENaC and δβγENaC. However, the amplitude of **PA1**-evoked photoswitching is higher on δβγENaC.

triggered a strong reduction in current. This effect could be reversed by switching back to 500 nm (Fig. 3 and Supplementary Fig. 4a). Thus, **PA1** functions as a *cis* blocker of δβγENaC. We found that the overall switching amplitude evoked by **PA1** is consistent between 1 and 10 μM and decided to settle on 10 μM as a working concentration, which provides maximal block in the *trans* state, close to a full amiloride block (Supplementary Fig. 4b). Control experiments using oocytes that expressed ENaC channels showed no innate sensitivity to light (Supplementary Fig. 5). Similarly, ENaC-expressing oocytes blocked by a 100 μM solution of amiloride did not respond to illumination[39].

Figure 3a shows the effect of **PA1** on a δβγENaC-mediated current. Wavelengths, and consequentially currents, were switched alternately in intervals of ten and five seconds. With light-mediated activation, perfusion-induced mechanical effects can be avoided, as recently demonstrated for ENaCs as well as for other members of the ENaC/deg family[40–43].

The photostationary state of azobenzenes, that is their *cis*/*trans* ratio, is a function of the illumination wavelength, which allows for controlling their effective concentrations with light. As a consequence, the degree to which δβγENaC channels are blocked by **PA1** also depends on the wavelength applied (Fig. 3b). Switching in 20 nm steps between a given wavelength and 500 nm results in a graded effect on the current. In line with our previous ultraviolet/visible (UV/vis) experiments, 400 nm radiation emerged as the most effective blocking wavelength. As shown in Fig. 3c, photoswitching mediated by 10 μM **PA1** could be detected on both αβγENaC- and δβγENaC-expressing oocytes. However, switching events were generally more robust and amplitudes were higher on δβγENaC (also see Supplementary Fig. 6).

PA1 photoswitching in human embryonic kidney cells. We next turned to human embryonic kidney (HEK293t) cells as a mammalian expression system. Given that these cells are smaller and transparent, we expected faster and more pronounced effects compared to those of the pigmented oocytes, for which only a fraction of the membrane surface can be illuminated. As depicted in Fig. 4, **PA1** is an excellent photoswitchable blocker of δβγENaC-expressing HEK cells. In line with the data from *Xenopus* oocytes, 400 nm radiation translates into a rapid block of ENaC currents, which can be released with 500 nm radiation (Fig. 4a). In the current-clamp mode, the action of **PA1** on δβγENaC translates into a pronounced and fast light-dependent change in membrane potential. Photoeffects are generally higher on the δβγ isoform over the tested range of 10 nM to 25 μM **PA1** and the difference between αβγENaC and δβγENaC increases with higher concentrations (Supplementary Fig. 6c,d). A comparison of photoswitching using HEK cells expressing either δβγENaC or αβγENaC and 10 μM **PA1** revealed that the average amplitude of the photocurrents is ~180 pA on the former and ~10 pA on the latter isoform. Similarly, the average change in membrane potential was ~57 mV and ~4 mV, respectively (Fig. 4b; overall expression was identical (Supplementary Fig. 8)). Thus, the general trends and effects that were found in *Xenopus* oocytes could also be observed in HEK cells, but much more pronounced and with a faster onset (Supplementary Fig. 7). We also found that *cis*-**PA1** thermally relaxes back to *trans*-**PA1** on a fast time scale (Fig. 4c). Thus, our novel optical tool can be operated by turning on and off a simple light source. As in the case of oocytes, intermediate wavelengths between 400 and 500 nm translate into graded effects (Fig. 4d). We were thus able to induce current and voltage steps in δβγENaC-expressing HEK cells by switching between 400, 433, 466 and 500 nm.

To determine further the potential of **PA1** as a tool for adjusting membrane potential, we set the starting potential in HEK cells in the current–clamp mode at −70 mV, initially using either blue or green illumination (Fig. 4e). Starting from these conditions, **PA1** can be used not only to hyperpolarize (switching from 500 to 400 nm), but also to depolarize (switching from 400 to 500 nm) a cell. As such, the δβγENaC–**PA1** system could be used as an optogenetic tool.

Pharmacokinetics of PA1 in HEK cells. In the course of our experiments using **PA1** on HEK cells expressing δβγENaC, we found that photoswitching is persistent and channel block remains after washout of **PA1** from the external recoding solution (Supplementary Fig. 9a,b). This interesting observation hints at a possible cell uptake or a reservoir formation in the cell membrane. Interestingly, *Xenopus* oocytes did not take up **PA1** as readily as HEK cells, which might be another reason for the difference in overall photoeffects (Supplementary Fig. 9c). To investigate this finding further, we preincubated coverslips with HEK cells expressing δβγENaC for one minute at room temperature in 10 μM **PA1**. Coverslips were then washed three

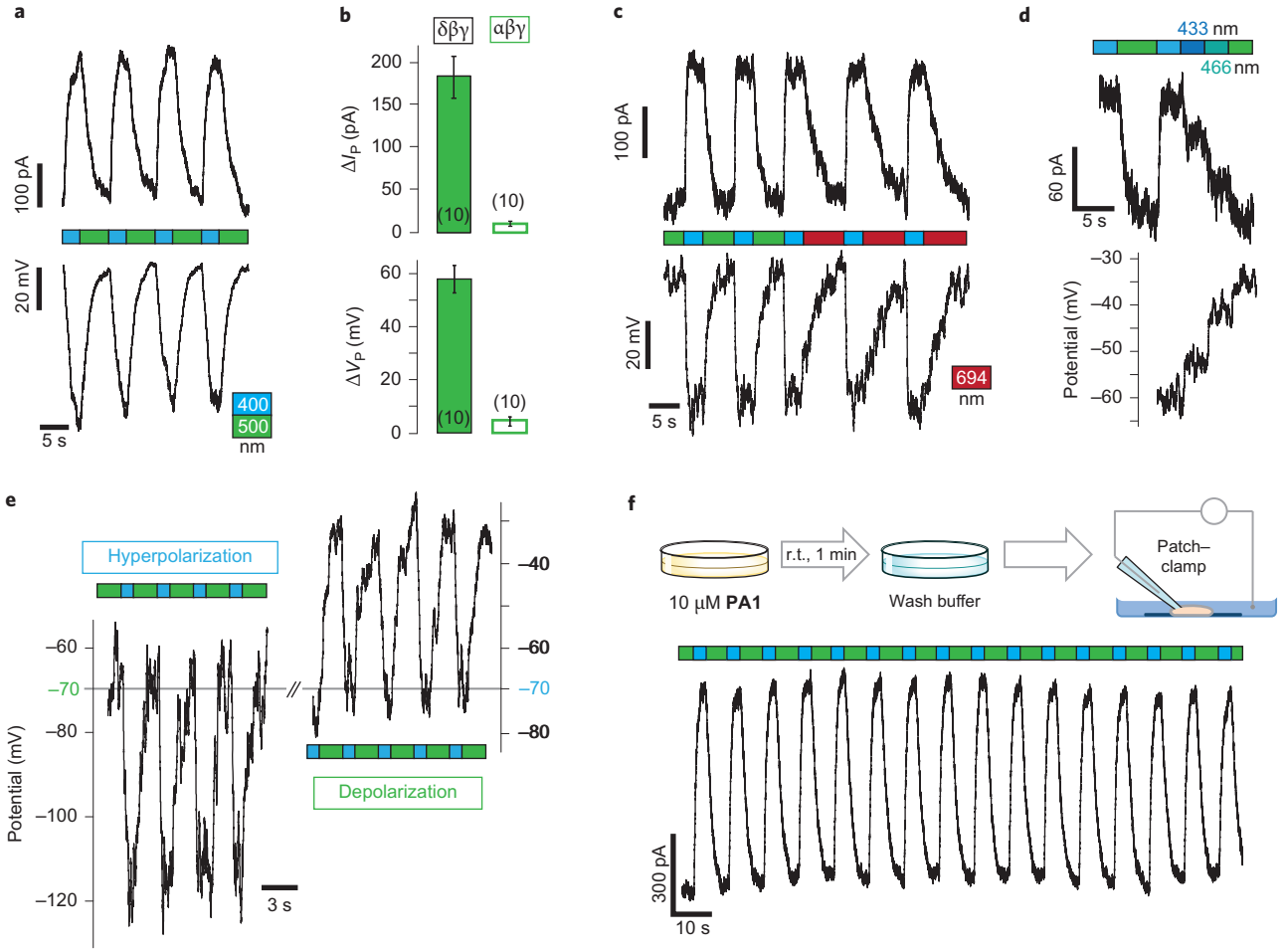

Figure 4 | Switching δβγENaC in HEK cells using 10 μM PA1. a, By switching between 400 and 500 nm both large currents (upwards deflection = inhibition) and potentials (downwards deflection = hyperpolarization) can be controlled by light. **b**, The average current amplitude of photoswitching (ΔI_P) is 182 pA for δβγENaC and 9 pA for αβγENaC. The average amplitude of the light-mediated membrane potential (ΔV_P) is 57 mV for δβγENaC and 4 mV for αβγENaC (currents and potentials were recorded from the same cell, $n = 10$ biological repeats from three independent transfections and holding potential was −60 mV). **c**, Comparison between light-induced and thermal relaxation. **d**, Application of light with wavelengths between 400 nm and 500 nm reveals the physiological action spectrum of **PA1** on δβγENaC-expressing HEK cells. Graded effects can be installed for both current (top) and membrane potential (bottom). **e**, Light-induced hyperpolarization and depolarization in the current-clamp mode. When the starting potential is adjusted to −70 mV under green light (left), photoswitching leads to hyperpolarization. When the starting potential is adjusted to −70 mV under blue light (right), photoswitching leads to depolarization. **f**, **PA1** can be loaded into HEK cells by a short incubation. After one minute incubation at room temperature (r.t.) in 10 μM **PA1** (yellow Petri dish) and subsequent wash (blue Petri dish), cells are ready for photoexperiments using the patch–clamp technique.

times and investigated using whole-cell patch–clamp experiments. We obtained a fully functional photoswitchable system with strong, persistent ENaC photocurrents (Fig. 4f). Figure 4f further demonstrates the rapid robust and reversible action of **PA1** on δβγENaC. Intriguingly, cells prepared in such a manner could be blocked and unblocked by amiloride without affecting photoswitching (Supplementary Fig. 10). However, photoswitching was reduced when phenamil was used as a blocker with similar lipophilicity, which is also taken up by cells (Supplementary Fig. 10c). In addition, we loaded **PA1** through the patch pipette (Supplementary Fig. 11). Photoswitching was possible instantaneously and a reversible amiloride block was also observed. Additional **PA1** delivered by perfusion did not enhance the photoeffect. These observations suggest that **PA1** finds its binding site from a membrane reservoir and has similar pharmacokinetics to long-lasting, use-dependent open channel blockers[44].

Use of PA1 in a lung-tissue model. With the ability of **PA1** to switch ENaC currents and to differentiate between αβγENaC and δβγENaC in HEK cells, we next wanted to employ **PA1** in a mammalian tissue model that endogenously expresses ENaC subunits. Human H441 bronchiolar epithelial cells were the model of choice because these cells (1) express all four ENaC subunits, including δENaC[16], and (2) form a polarized epithelium, which allows the electrophysiological assessment of sodium transport across an intact cell monolayer. Furthermore, despite the molecular evidence for δENaC expression in pulmonary epithelia, a functional contribution of this isoform to transepithelial sodium transport has not been demonstrated[22].

To address the functional role of δβγENaC in these cells, we measured the transepithelial potential of H441 monolayers, which were cultured on permeable membrane supports (Fig. 5a). First, we determined the magnitude of the overall amiloride-sensitive transepithelial potential (V_E) (on average ~4 mV, Fig. 5c). We then exchanged the apical bath solution for 10 μM **PA1** and switched between 400 and 500 nm, and 400 nm and 694 nm for three cycles, respectively (Fig. 5b). The deep-red wavelength functionally corresponds to darkness because our

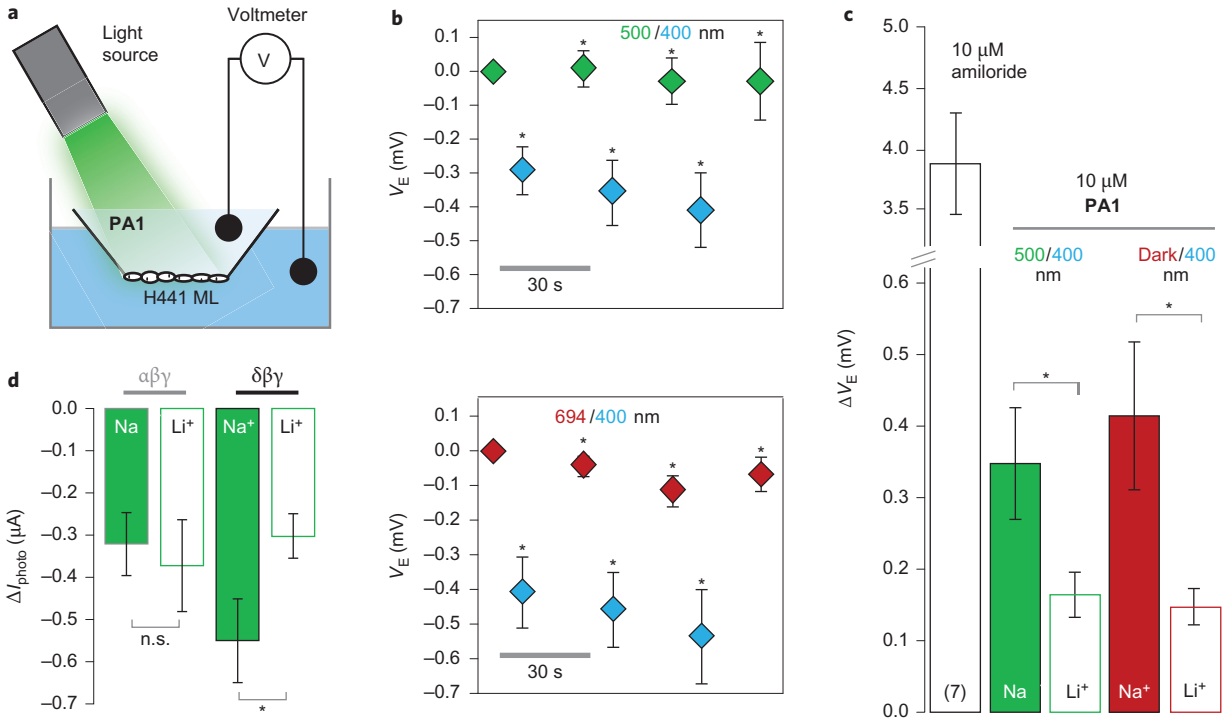

Figure 5 | Photocontrol of transepithelial potential in H441 monolayers. a, Experimental configuration with an H441 monolayer (ML) on a filter inlet. The apical compartment contained 10 µM **PA1** in sodium- or lithium-based buffer and was illuminated with a monochromator. The transepithelial potential V_E between the apical and basolateral compartment was measured by a voltmeter (apical electrode is the reference). **b**, V_E can be switched by toggling between 500 nm and 400 nm radiation (top), as well as between 694 nm and 400 nm (bottom). The 400 nm radiation was applied for ten seconds, the longer wavelengths for 20 seconds and the voltage was recorded at the end of each illumination period. Photoeffects are robust and reversible for both protocols. **c**, Comparison of the entire amiloride-sensitive V_E and **PA1**-mediated photosensitive V_E with apical sodium or lithium using both 400/500 nm and 400 nm/dark switching ($n = 7$). **d**, Comparison of the effect of extracellular lithium on αβγENaC and δβγENaC photocurrents in *Xenopus* oocytes ($n \geq 7$). Error bars indicate s.e.m., $^*p$-value < 0.05.

azobenzenes do not absorb in this region. Results were identical for the different wavelength protocols and the overall magnitude was a photosensitive transepithelial potential V_E of ~0.4 mV (Fig. 5b). This finding hints towards a small amount of functional δβγENaC. To investigate whether the photoeffect comes from δβγENaC or is a small effect of αβγENaC, we addressed the lithium conductivity of each isoform. The ratio between lithium and sodium conductivity is 0.64 for δβγENaC and 2.0 for αβγENaC[22]. Thus, we expected decreased photoeffects for the δ-containing isoform and increased effects for the α-containing isoform when sodium is replaced by lithium. We confirmed this hypothesis using *Xenopus* oocytes (Fig. 5d), which had shown photoeffects for either isoform before. Similarly, δβγENaC photocurrents were significantly reduced in HEK cells by extracellular lithium (Supplementary Fig. 12). When sodium was substituted by lithium at the apical side of the H441 monolayer, **PA1**-mediated photoeffects decreased from 0.4 to 0.15 mV for both wavelength protocols (Fig. 5c). Thus, the photosensitive fraction of V_E results from δβγENaC rather than from αβγENaC. These data strongly indicate a functional expression of δβγENaC in H441 cells and underline the ability of **PA1** for functional differentiation between αβγENaC and δβγENaC.

Conclusion

In summary, the photoswitchable ENaC blocker **PA1** has been designed, synthesized and functionally characterized using electrophysiology with *Xenopus* oocytes, HEK293t cells and H441 cell monolayers. Our results provide new insights into the structure–activity relationships of the amiloride class of diuretics and outline a strategy to address selectively the αβγ and δβγ isoforms of ENaC channels. **PA1** can be used to control δβγENaCs optically by switching between blue and green light, or by turning on and off blue light. This therefore allows ENaC to be investigated without mechanical stress. We showed that **PA1** is long lasting and can be applied by perfusion, cell incubation or loading through the patch pipette. We used **PA1** to address the significance of different ENaC isoforms in H441 monolayers and identified functional δβγENaC. The combination of photoswitchable **PA1** and the voltage-insensitive δβγENaC is a powerful tool to control precisely the membrane potential with light, allowing for both hyper- and depolarization. With its unique functional profile, **PA1** could enable new insights into the δβγENaC function, for instance in the primate brain.

Methods

The Supplementary Information gives details of chemical syntheses and *Xenopus* oocytes cultures.

Cell culture and electrophysiology. HEK293t cells were cultured in DMEM buffer with 10% fetal bovine serum in a 10% CO_2 37 °C incubator. At 90–95% confluency, cells were split and used for transient transfection using the jetPRIME polyplus transfection reagent in accordance with the supplier's protocol. Poly-L-lysine-coated acid-etched glass coverslips were placed in a 24-well plate and consecutively treated with the DNA mix (150 ng of each ENaC subunit and 50 ng yellow fluorescent protein (YFP)) and 30,000 to 50,000 cells in growth medium. After 2–4 hours, the supernatant was removed and growth medium supplemented with 10 µM amiloride was added. Cells were used for electrophysiological recordings 12–48 hours post-transfection. Only YFP-positive cells with an amiloride-sensitive current were used for the experiments. For each repeat, a new cover slip was used.

Whole-cell patch–clamp experiments were performed using a standard electrophysiology set-up equipped with a HEKA Patch Clamp EPC10 USB amplifier and PATCHMASTER software. Micropipettes were generated from Science

Products GB200-F-8P with filament pipettes using a vertical puller. Resistance varied between 5 and 8 MΩ. The bath solution contained (in mM) 140 NaCl (or LiCl), 3 KCl, 2 $CaCl_2$, 1 $MgCl_2$, 10 D-glucose, 20 HEPES (NaOH to pH 7.4). The pipette solution contained (in mM): 90 K gluconate, 10 NaCl, 10 KCl, 1 $MgCl_2$, 10 EGTA, 60 HEPES (KOH to pH 7.3). Photoswitchable ligands and reference agonist were dissolved in bath solution from a 1,000× DMSO stock.

H441 cells were purchased from American Type Culture Collection in the 65th passage and cultured under liquid/air conditions in the presence of 200 nM dexamethasone, as previously described[45]. For the experiments, H441-containing cell culture inserts were placed in six-well plates containing H441 saline (2 ml in the basolateral compartment and 500 µl in the apical compartment). H441 saline contained (in mM): 130 NaCl (or LiCl), 2.7 KCl, 1.5 KH_2PO_4, 1 $CaCl_2$, 0.5 $MgCl_2$, 10 HEPES, 10 glucose (37 °C, pH 7.35 (TRIZMA)). V_E was measured with an epithelial voltohmmeter (EVOM, World Precision Instruments). The shorter electrode was placed in the apical compartment and served as reference. When V_E was stable, amiloride was added to the apical compartment to a final concentration of 100 µM to investigate the amiloride-sensitive fraction of V_E. Monolayers were washed three times with H441 saline and afterwards 10 µM **PA1** was added to the apical compartment. When V_E stabilized again, the EVOM was zeroed (for better comparability between cell preparations) and monolayers were exposed to different wavelengths. Afterwards, cells were rinsed with lithium-containing saline and the same measurement protocol was employed. Experiments were performed at 37 °C on seven H441 monolayers from two independent cell preparations.

Irradiation was performed on a TILL Photonics Polychrome 5000 monochromator. In patch–clamp experiments, the light beam was guided through the microscope objective and operated by the amplifier and PATCHMASTER software. In all other experiments, a light fibre was positioned in proximity to the object of interest and the monochromator was operated using the POLYCON 3.1 software.

Received 7 May 2013; accepted 12 June 2014; published online 20 July 2014

References

1. Alvarez de la Rosa, D., Canessa, C. M., Fyfe, G. K. & Zhang, P. Structure and regulation of amiloride-sensitive sodium channels. *Ann. Rev. Physiol.* **62,** 573–594 (2000).
2. Canessa, C. M., Merillat, A. M. & Rossier, B. C. Membrane topology of the epithelial sodium channel in intact cells. *Am. J. Physiol.* **267,** C1682–C1690 (1994).
3. Canessa, C. M. *et al.* Amiloride-sensitive epithelial Na^+ channel is made of three homologous subunits. *Nature* **367,** 463–467 (1994).
4. Bubien, J. K. Epithelial Na^+ channel (ENaC), hormones, and hypertension. *J. Biol. Chem.* **285,** 23527–23531 (2010).
5. Chang, S. S. *et al.* Mutations in subunits of the epithelial sodium channel cause salt wasting with hyperkalaemic acidosis, pseudohypoaldosteronism type 1. *Nature Genet.* **12,** 248–253 (1996).
6. Boucher, R. C. New concepts of the pathogenesis of cystic fibrosis lung disease. *Eur. Respir. J.* **23,** 146–158 (2004).
7. Hummler, E. *et al.* Early death due to defective neonatal lung liquid clearance in αENaC-deficient mice. *Nature Genet.* **12,** 325–328 (1996).
8. Scherrer, U. *et al.* High-altitude pulmonary edema: from exaggerated pulmonary hypertension to a defect in transepithelial sodium transport. *Adv. Exp. Med. Biol.* **474,** 93–107 (1999).
9. Althaus, M., Clauss, W. G. & Fronius, M. Amiloride-sensitive sodium channels and pulmonary edema. *Pulm. Med.* **2011,** 830320 (2011).
10. Althaus, M. ENaC inhibitors and airway re-hydration in cystic fibrosis: state of the art. *Curr. Mol. Pharmacol.* **6,** 3–12 (2013).
11. Fronius, M. Treatment of pulmonary edema by ENaC activators/stimulators. *Curr. Mol. Pharmacol.* **6,** 13–27 (2013).
12. Bull, M. B. & Laragh, J. H. Amiloride: a potassium-sparing natriuretic agent. *Circulation* **37,** 45–53 (1968).
13. Schoenberger, M. & Althaus, M. Novel small molecule epithelial sodium channel inhibitors as potential therapeutics in cystic fibrosis – a patent evaluation. *Expert Opin. Therapeut. Patents* **23,** 1383–1389 (2013).
14. Waldmann, R., Champigny, G., Bassilana, F., Voilley, N. & Lazdunski, M. Molecular cloning and functional expression of a novel amiloride-sensitive Na^+ channel. *J. Biol. Chem.* **270,** 27411–27414 (1995).
15. Giraldez, T. *et al.* Cloning and functional expression of a new epithelial sodium channel delta subunit isoform differentially expressed in neurons of the human and monkey telencephalon. *J. Neurochem.* **102,** 1304–1315 (2007).
16. Wesch, D. *et al.* Differential N termini in epithelial Na^+ channel delta-subunit isoforms modulate channel trafficking to the membrane. *Am. J. Physiol. Cell Physiol.* **302,** C868–879 (2012).
17. Teruyama, R., Sakuraba, M., Wilson, L. L., Wandrey, N. E. & Armstrong, W. E. Epithelial Na^+ sodium channels in magnocellular cells of the rat supraoptic and paraventricular nuclei. *Am. J. Physiol. Endocrinol. Metab.* **302,** E273–E285 (2012).
18. Ji, H.-L. *et al.* δENaC: a novel divergent amiloride-inhibitable sodium channel. *Am. J. Physiol. Lung Cell. Mol. Physiol.* **303,** L1013–L1026 (2012).
19. Yamamura, H., Ugawa, S., Ueda, T., Nagao, M. & Shimada, S. A novel spliced variant of the epithelial Na^+ channel delta-subunit in the human brain. *Biochem. Biophys. Res. Commun.* **349,** 317–321 (2006).
20. Miller, R. L., Wang, M. H., Gray, P. A., Salkoff, L. B. & Loewy, A. D. ENaC-expressing neurons in the sensory circumventricular organs become c-Fos activated following systemic sodium changes. *Am. J. Physiol. Regul. Integr. Comp. Physiol.* **305,** R1141–R1152 (2013).
21. Giraldez, T., Dominguez, J. & Alvarez de la Rosa, D. ENaC in the brain – future perspectives and pharmacological implications. *Curr. Mol. Pharmacol.* **6,** 44–49 (2013).
22. Giraldez, T., Rojas, P., Jou, J., Flores, C. & Alvarez de la Rosa, D. The epithelial sodium channel δ-subunit: new notes for an old song. *Am. J. Physiol. Renal Physiol.* **303,** F328–F338 (2012).
23. Kellenberger, S. & Schild, L. Epithelial sodium channel/degenerin family of ion channels: a variety of functions for a shared structure. *Physiol. Rev.* **82,** 735–767 (2002).
24. Jasti, J., Furukawa, H., Gonzales, E. B. & Gouaux, E. Structure of acid-sensing ion channel 1 at 1.9 Å resolution and low pH. *Nature* **449,** 316–23 (2007).
25. Fehrentz, T., Schonberger, M. & Trauner, D. Optochemical genetics. *Angew. Chem. Int. Ed.* **50,** 12156–12182 (2011).
26. Banghart, M., Borges, K., Isacoff, E., Trauner, D. & Kramer, R. H. Light-activated ion channels for remote control of neuronal firing. *Nature Neurosci.* **7,** 1381–1386 (2004).
27. Mourot, A. *et al.* Rapid optical control of nociception with an ion-channel photoswitch. *Nature Methods* **9,** 396–402 (2011).
28. Volgraf, M. *et al.* Allosteric control of an ionotropic glutamate receptor with an optical switch. *Nature Chem. Biol.* **2,** 47–52 (2006).
29. Levitz, J. *et al.* Optical control of metabotropic glutamate receptors. *Nature Neurosci.* **16,** 507–516 (2013).
30. Tochitsky, I. *et al.* Optochemical control of genetically engineered neuronal nicotinic acetylcholine receptors. *Nature Chem.* **4,** 105–111 (2012).
31. Cragoe, E. J., Woltersd. O. W., Bicking, J. B., Kwong, S. F. & Jones, J. H. Pyrazine diuretics. 2. *N*-amidino-3-amino-5-substituted L-halopyrazinecarboxamides. *J. Med. Chem.* **10,** 66–75 (1967).
32. Kleyman, T. R. & Cragoe, E. J. Jr. Amiloride and its analogs as tools in the study of ion transport. *J. Membr. Biol.* **105,** 1–21 (1988).
33. Cuthbert, A. W., Fanelli, G. M. & Scriabine, A. *Amiloride and Epithelial Sodium Transport* (Urban & Schwarzenberg, 1979).
34. Li, J. H., Cragoe, E. J. Jr & Lindemann, B. Structure–activity relationship of amiloride analogs as blockers of epithelial Na channels: II. Side-chain modifications. *J. Membr. Biol.* **95,** 171–185 (1987).
35. Garvin, J. L., Simon, S. A., Cragoe, E. J. Jr & Mandel, L. J. Phenamil: an irreversible inhibitor of sodium channels in the toad urinary bladder. *J. Membr. Biol.* **87,** 45–54 (1985).
36. Hirsh, A. J. *et al.* Design, synthesis, and structure–activity relationships of novel 2-substituted pyrazinoylguanidine epithelial sodium channel blockers: drugs for cystic fibrosis and chronic bronchitis. *J. Med. Chem.* **49,** 4098–4115 (2006).
37. Sadovski, O., Beharry, A. A., Zhang, F. & Woolley, G. A. Spectral tuning of azobenzene photoswitches for biological applications. *Angew. Chem. Int. Ed.* **48,** 1484–1486 (2009).
38. Mourot, A. *et al.* Tuning photochromic ion channel blockers. *ACS Chem. Neurosci.* **2,** 536–543 (2011).
39. Pulgarin, J. A. M., Molina, A. A. & Lopez, P. F. Direct analysis of amiloride and triamterene mixtures by fluorescence spectrometry using partial-least squares calibration. *Anal. Chim. Acta* **449,** 179–187 (2001).
40. Althaus, M., Bogdan, R., Clauss, W. G. & Fronius, M. Mechano-sensitivity of epithelial sodium channels (ENaCs): laminar shear stress increases ion channel open probability. *FASEB J.* **21,** 2389–2399 (2007).
41. Fronius, M., Bogdan, R., Althaus, M., Morty, R. E. & Clauss, W. G. Epithelial Na^+ channels derived from human lung are activated by shear force. *Respir. Physiol. Neurobiol.* **170,** 113–119 (2010).
42. Geffeney, S. L. *et al.* DEG/ENaC but not TRP channels are the major mechanoelectrical transduction channels in a *C. elegans* nociceptor. *Neuron* **71,** 845–857 (2011).
43. Kim, E. C., Choi, S. K., Lim, M., Yeon, S. I. & Lee, Y. H. Role of endogenous ENaC and TRP channels in the myogenic response of rat posterior cerebral arteries. *PLoS One* **8,** e84194 (2013).
44. Scholz, A. Mechanisms of (local) anaesthetics on voltage-gated sodium and other ion channels. *Br. J. Anaesth.* **89,** 52–61 (2002).
45. Althaus, M. *et al.* Nitric oxide inhibits highly selective sodium channels and the Na^+/K^+-ATPase in H441 cells. *Am. J. Respir. Cell Mol. Biol.* **44,** 53–65 (2011).

Acknowledgements

We thank the European Research Commission for an ERC Advanced Grant (Grant No. 268795 to D.T.). M.A. is supported by grants from the German Research Foundation

(AL1453/1-1 and AL1453/1-2), M.F. and W.C. acknowledge a grant provided by the Federal State of Hesse (LOEWE Research Focus, Non-neuronal cholinergic systems). M.S. was supported by a grant from the German Study Foundation and the International Max Planck Research School (IMPRS-LS). We acknowledge the support of K. Hüll (chemical synthesis) and L. de la Osa de la Rosa (cell-culture work), and we thank D. Barber for helpful comments. We also thank D. Alvarez de la Rosa for providing constructs of all ENaC subunits in pcDNA3.1.

Author contributions

D.T., M.A., M.S. and M.F. conceived the study and designed the experiments. M.S. performed the chemical synthesis and UV/vis characterization. M.S. and M.A. performed the electrophysiological characterization. D.T. and W.C. supervised the study and wrote the paper, together with M.S., M.F. and M.A.

Additional information

Supplementary information and chemical compound information is available in the online version of the paper. Reprints and permissions information is available online at www.nature.com/reprints. Correspondence and requests for materials should be addressed to D.T.

Competing financial interests

The authors declare no competing financial interests.